Primary Mirror Segment Fabrication for CELT

Terry S. Mast[a], Jerry E. Nelson[a], and Gary E. Sommargren[b]

a. University of California Observatories / Lick Observatory
University of California, Santa Cruz, CA 95064
mast@ucolick.org (831.459.3807), jnelson@ucolick.org (831.459.5132)
b. Lawrence Livermore National Laboratory, Livermore, CA 94550
sommargren@llnl.gov (925.423.8599)

ABSTRACT

The primary mirror of the proposed California Extremely Large Telescope (CELT) is a 30-meter diameter mosaic of hexagonal segments. An initial design calls for about a thousand segments with a hexagon side length of 0.5 meters, a primary-mirror focal ratio of 1.5, and a segment surface quality of about 20 nanometers rms. We describe concepts for fabricating these segments.

Keywords: CELT, California Extremely Large Telescope, primary mirror, segment fabrication, large optics

Contents

1. CELT OVERVIEW

We are designing a 30-meter-diameter telescope for astronomy at visible and infrared wavelengths. The project is a collaboration of the University of California and the California Institute of Technology, and the telescope is currently named the California Extremely Large Telescope (CELT). The project overview is given in another paper at this conference (Design Concepts for the California Extremely Large Telescope (CELT) (Nelson, 2000)) and in a series of internal project reports.

The telescope optical design calls for Ritchey-Chretien foci with the following parameters. For comparison we also list design parameters for the W. M. Keck telescopes.

	CELT	Keck
primary diameter (m)	30	10
primary focal ratio	1.50	1.75
backfocal distance (m)	15.00	2.5
primary radiius of curvature (m)	90.000	35.000
primary conic constant	−1.0028	−1.003683
secondary radius of curvature (m)	−12.12	−4.738
secondary conic constant	−1.525	−1.644
final focal length (m)	450	150

The focal ratio of the primary (1.50) was chosen as a compromise between minimizing the segment asphericity (minimizing the segment fabrication costs) and minimizing the size of the dome (a significant fraction of the observatory cost).

The large primary mirror will be segmented and the piston/tip/tilt degrees of freedom of each segment will be under active control. The segmentation geometry is discussed below. Other papers at this conference discuss the sensors and actuators for active control (Segmented Mirror Control System Hardware for CELT, Mast and Nelson, 2000) and the control system design (Design Issues for the Active Control System of the California Extremely Large Telescope (CELT), Chanan *et al.* , 2000).

To place the surface fabrication in perspective we note the following telescope primary optical surface areas:

Hale Telescope	20 meter^2
Two Keck Telescopes	150 meter^2
Four VLT Telescopes	210 meter^2
CELT	700 meter^2

The increase in primary mirror diameter from 10 meters to 30 meters is a challenging advance. In order to begin construction in two to three years, we believe that major innovations in technology will not be possible. The emphasis of the development and innovation for this project will be directed toward reducing costs of largely existing technologies.

2. SEGMENT DESIGN OPTIONS

The selection of a segment size, and hence the number of segments, depends on a complex tradeoff of many costs. A larger segment size (radius = a, thickness = h) increases the amount of asphericity required in the surface figure ($\sim a^2$), the gravity-induced deflections on a support, ($\sim a^4 / h^2$) , the weight for handling ($\sim a^2$ h), and sensitivity to position errors in the array ($\sim a^2$). A smaller segment size increases the number of active control actuators and sensors, the complexity of a control wavefront sensor, and the complexity of the alignment and control software.

The selection of the segment thickness is also a complex compromise between costs. A larger thickness will require larger required forces for intentional deformation during fabrication, greater cost of the blank material, greater thermal inertia in the telescope, and a greater mass for the support structure (the telescope). A smaller thickness will require more support points to reduce deformations due to gravity.

At this early phase of the design we have not yet gathered estimates of these costs and cost variations, This will be required to make final informed compromises. Based on our experience with the Keck telescopes, we have adopted for now a baseline segment design. During the coming phases this will evolve to final values for the radius and thickness. In the meantime we have adopted a segment radius of a = 0.5 meters and a segment thickness of h = 45 millimeters.

The resulting array (Figure 1) contains 1080 segments. A central subset of 19 segments is deleted from the array since the light to them is blocked by the secondary mirror.

We have the option of adjusting the positions of some peripheral segments to keep a closely circular periphery and at the same time to allow for convenient division of the array into subsets (full and partial "rafts" of 19 segments) for ease of handling. The array shown in Figure 1 has an area = 702 m^2.
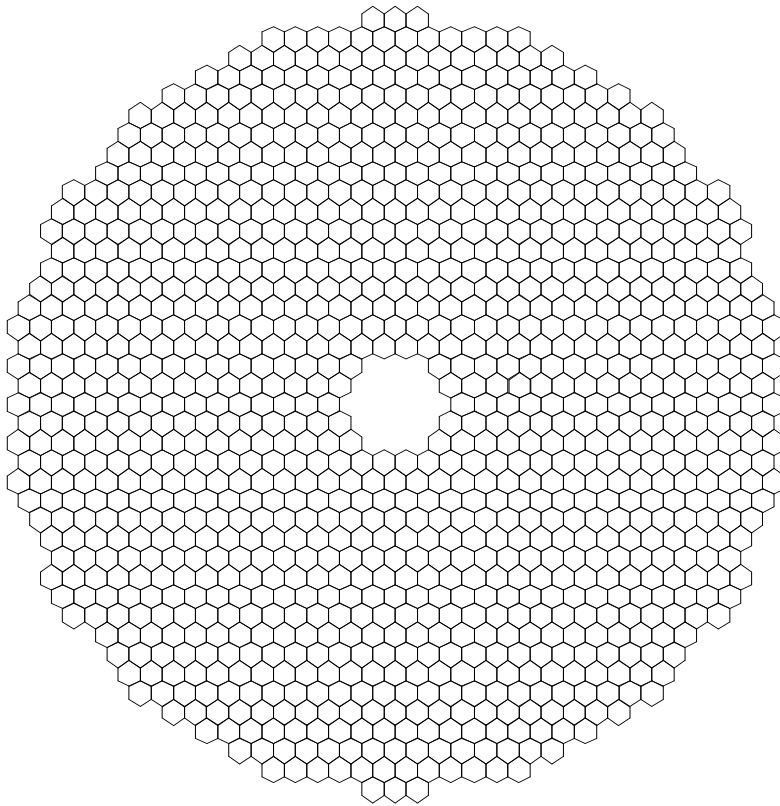
Figure 1. Segmentation option for the CELT primary mirror containing 1080 segments.

3. SEGMENT SPECIFICATIONS

Based on our assumed baseline for the telescope optical design and primary mirror segmentation geometry, we can calculate the surface figure of each segment. We describe these in terms of an expansion in Zernike polynomials (Nelson, Gabor, Hunt, Lubliner, and Mast, 1980). Each coefficient is a function of R = the off-axis distance of the segment center, k = primary mirror radius of curvature, K = the conic constant, and $\rho = r/a$ (where r = segment radial coordinate and a = segment radius). The segment surface in a coordinate system centered on the segment, with the z axis normal to the surface is given by $z(\rho,\theta) = \Sigma\ C_{ij}\ Z_{ij}\ (\rho,\theta)$. To lowest order in R/k, the dominant terms are

$$Z_{20} = \quad 2\rho^2 - 1 \qquad\qquad C_{20} = a^2/(4k) + Ka^2R^2/(4k^3) + \ldots \qquad\qquad (1)$$

$$Z_{22} = \quad \rho^2 \cos 2\theta \qquad\qquad C_{22} = Ka^2 R^2/(4k^3) + \ldots \qquad\qquad (2)$$

$$Z_{31} = \quad (3\rho^3 - 2\rho)\ \cos\theta \qquad\qquad C_{31} = K\ a^3\ R/(6k^3) + \ldots \qquad\qquad (3)$$

For k = 90 m and a = 0.5 m these coefficients are plotted as a function of R in Figure 2.
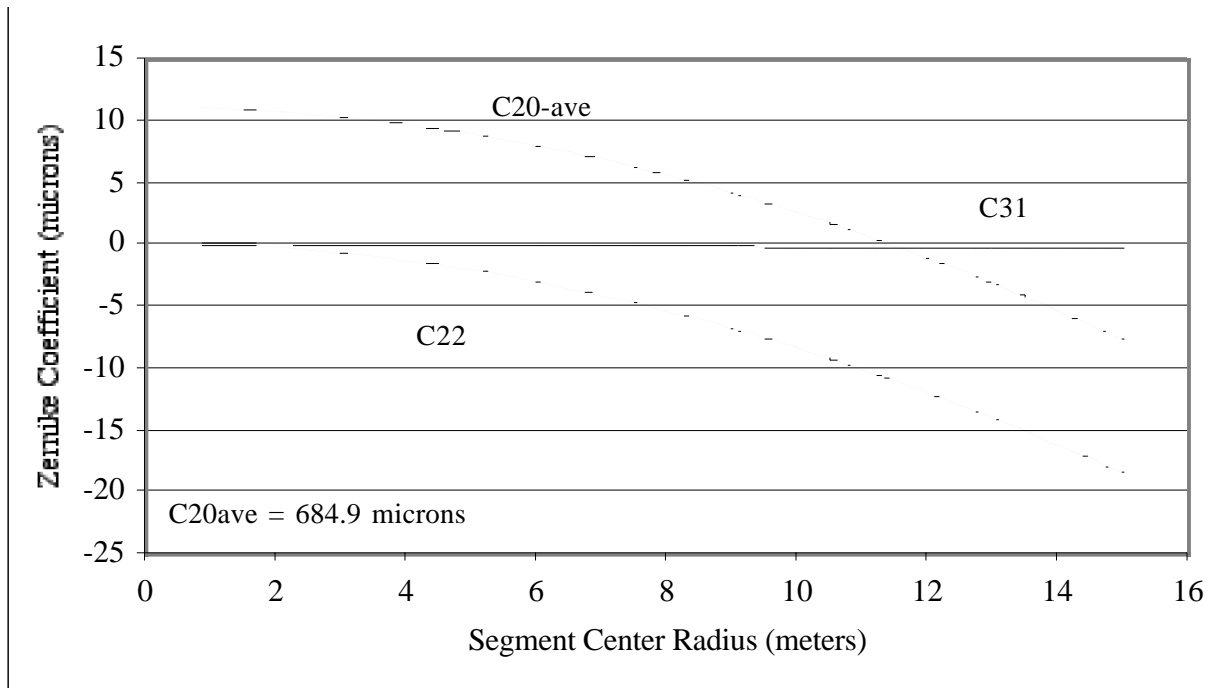
Figure 2. Segment surface Zernike Coefficients (microns) versus segment-center radius (m).

C_{20} varies over the range 694.4 to 675.7 microns. The outermost segment deviates most from a sphere; the coefficients for the outermost segment are

	CELT	**Keck**
a (meters)	0.5	0.9
R (meters)	15	4.68
$C_{20} - C_{20}$ on axis	−19	−100
C_{22} (microns)	−19	−100
C_{31} (microns)	−0.4	−13.

Our baseline design for the mechanical shape of the segments assumes a 2.0 mm gap between segments. We assume the sides of the hexagonal prism are parallel to the local normal to the primary surface at the segment center. We also assume the back surface of the segment is a convex sphere with a radius = 91 meters for all segments (the average front-side radius). With an assumed bevel of 1 mm, the non-reflecting gap is 4 mm. There are 3102 inter-segment gaps with a total fractional light-loss area of 0.0088. For comparison, the Keck segments are separated by 3 mm gaps and have 2 mm bevels; resulting in a fractional light-loss area = 0.0070.

A full error budget for the telescope is being constructed. The primary mirror component of that budget will contain terms for surface figuring, gravity deformations, thermal distortion, alignment-passive, and alignment-active. The surface figuring budgeted error has two contributions; focal length errors (δC_{20}) and higher-order surface errors (δC_{22} and above). This separation is motivated by the different measurement techniques used to control these. We adopt here some interim estimates. For surface figuring we budget 20 nm rms total surface error and assume $S_{rms} = 14$ nm rms for each of the two terms. The rms C_{20} coefficient variation δC_{20} corresponding to an rms surface variation is $\delta C_{20} = S_{rms} / 0.510$ (over a hexagon). An rms variation δC_{20} in the C_{20} coefficient corresponds to an rms error in the radius of curvature $\delta k = (4k^2 / a^2) \delta C_{20}$. The geometric optics image blur can be described by the 80%-enclosed-energy diameter and from a hexagonal mirror $\theta(80)$ (arc sec) $= 13.3 \; \delta C_{20} / a$.

For $S_{rms} = 14$ nm, $\qquad \delta C_{20} = 27$ nm rms and $\delta k = 3.5$ mm rms and $\theta(80) = 0.148$ arc seconds on the sky.
If the entire higher-order surface error (14 nm rms surface) was due to δC_{22}, then
$\delta C_{22} = S_{rms} / 0.357 = 39$ nm and $\theta(80) = 6.64 \; \delta C_{22} / a = 0.11$ arc seconds on the sky.

4. KECK SEGMENT FABRICATION REVIEW

CELT will necessarily use a segmented primary mirror. To date the only large segmented mirrors in use are those in the Keck telescopes and in the Hobby-Eberly telescope (HET). Because the HET segments have spherical surfaces we use the Keck segment fabrication as a basis for studying options for CELT. The Keck segment fabrication process is summarized in the table below. The Keck segments were polished by Itek Optical Systems (Lexington, MA) and Tinsley Laboratories (Richmond, CA). The ion figuring was done by Eastman Kodak (Rochester, NY). The testing method used during or after each process step is indicated.

Process Flow	**Testing**
Convex Side Polish	Spherometer
|	
Stressed Mirror Grind and Polish	Profilometer
|	Autocollimation Test
Cut Hexagon	
|	
Drill Holes for Support	
|	Autocollimation Test
Ion Figure	
|	Autocollimation Test
Mount on Support	
|	
Install in Telescope	
|	Hartmann-Shack Test
Set Warping Harness (in telescope)	
|	Hartmann-Shack Test

Stressed Mirror Polishing includes the following major steps:
1. Apply shear forces and moments at the edge of the circular blank using 24 levers.to elastically deform the blank to induce a surface equal to [polished-sphere minus desired-hyperboloid]. This required forces = 0 to 15 kg and moments = 26 to 46 kg-m per lever.
2. Polish a sphere into the deformed blank.
3. Release the forces and moments, and the blank elastically relaxes, and the sphere deforms into the desired hyperboloid.

Warping Harness refers to a system of 30 leaf springs integrated with the axial support on the back of each segment. These are used to achieve the final segment figure based on in-telescope measurements using a Hartmann-Shack test and a bright star.

5. SEGMENT BLANK OPTIONS

Before a final selection of blank material is made we will study the costs and performance of various candidates. We are considering Zerodur (Schott Optical Technologies, Mainz, Germany), ULE fused silica (Corning Corporation, Canton, NY), aluminum, and composites.

The issues that will be studied in order to make an informed decision include technology development required, internal stress that may cause unpredictable warping from cutting, polishability, support complexity, mass of support structure, stiffness-to-weight ratio, thermal stability, and material cost.

We are also considering two options for the initial blank shape; circular and hexagonal.

We list below a baseline set of blank specifications.

baseline set of blank specifications

	CELT	Keck
circular blank diameter (m)	1.05	1.9
meniscus uniform thickness (mm)	45	75
meniscus surface radius of curvature	91 meters	35 meters
stress birefringence mean less than	3 nm/cm	3 nm/cm
coefficient thermal expansion		
mean (rms) =	$1.0\ (2.0)\ \text{x}10^{-8}\ /\ ^{\text{o}}\text{C}$	$1.0\ (2.0)\ \text{x}10^{-8}\ /\ ^{\text{o}}\text{C}$
coefficient of thermal expansion axial variation through thickness		
mean (rms) =	$1.7\ (2.2)\ \text{x}10^{-9}\ /\ ^{\text{o}}\text{C}$	$1.7\ (2.2)\ \text{x}10^{-9}\ /\ ^{\text{o}}\text{C}$
segment mass	74 kg	400 kg

6. SEGMENT FIGURING OPTIONS

The final figure of the Keck segments was achieved using Stressed-Mirror Polishing, Ion Figuring, and Warping Harnesses. For CELT we believe some combination of these processes can be used to figure the segments. Other processes, such as replication and diamond turning, are also potential candidates. At this writing the state of development of replication and the specificity of diamond turning to metal mirrors, suggest these may be less attractive options. In this report we describe only our initial investigations, which are focussed on the three processes used for Keck.

Planetary Stressed Mirror Polishing

For the large number of segments envisioned for CELT we believe a modification of stressed-mirror polishing will be required for economical fabrication. One attractive option for this modification would be to figure several segments simultaneously using planetary polishing. With a stressing fixture above and attached to the edges of each blank, the initial polished out surface will be close to the asphere required.

For a baseline design we have assumed a 1.05 meter diameter circular blank and calculated the forces and moments required to deform it for Stressed Mirror Polishing.

We have first used analytic calculations to calculate the approximate sizes of forces and moments required to achieve the required aspheres. We then have used a finite-element code to calculate more accurate values.

Our analytic estimate is based on Lubliner and Nelson (1979). The axial force density $V(\theta)$ and moment density $M(\theta)$ around the edge of a circular blank required to achieve given values of C_{20} and C_{22} are given below. We neglect here the need for a small C_{31} but it can be readily included.

$$M(\theta) = M_0 + M_2 \cos(2\theta) \qquad\qquad V(\theta) = V_0 + V_2 \cos(2\theta) \qquad (4)$$

And
$$M_0 = (D/a^2)\ (2 + \nu)\ 2\ \delta C_{20} \qquad\qquad V_0 = 0 \qquad (5)$$
$$M_2 = (D/a^2)\ (1 - \nu)\ 2\ \delta C_{22} \qquad\qquad V_2 = M_2\ (2/a) \qquad (6)$$

where $\quad D = Eh^3\ /[12(1-\nu^2)]$ and h is the blank thickness. $\qquad (7)$

The units are $[M] = N$, $[V] = N/m$, $[E] = N/m^2$, $[h] = m$

For the design described above $\qquad E = 9.06\text{E}+10\ \text{N}/m^2$, $\nu = 0.24$, $a = 0.525$ m, $h = 0.045$ m,

Equations 5 to 7 yield $\qquad D = 7.3\text{E}+5$ N-m $\quad M_0 = 1.19\text{E}+7\ \delta C_{20} \qquad M_2 = 4.03\text{E}+6\ \delta C_{22}$

For the outermost segment $R = 15.0$ m ,

$\qquad \delta C_{20} = -9.2$ microns (assumes planetary tool radius $\sim C_{20}$ ave = 684.9 microns)

$\qquad \delta C_{22} = -18.6$ microns.

These imply $\qquad M_0 = 109$ N $\qquad M_2 = 75$ N $\qquad V_2 = 286$ N/m

This analytic estimate assumes the blank is a thin plate. For a more accurate model that includes the effects of the finite thickness of the blank and shear stresses, we have begun a finite-element calculation using the program ANSYS. Since a finite number levers are used in practice (24 for Keck), there are high-spatial-frequency local deformations at the edge of the

blank where the forces and moments are applied. Most of these are removed when the circular blank is cut into a hexagon. The finite element calculation will be used to estimate these local effects and will contribute to determining the optimal radius of the circular blank and the required density of levers.

We have begun to address the practical issues in planetary polishing. Today there exist three large planetary polishing machines in the United States with diameters of 3.7, 4.1, and 4.6 meters. We have not yet learned of the applicability, availability, and costs of these polishers for the CELT segments. The very large number of segments may warrant the fabrication of a new polisher specifically designed for this fabrication program.

Ion Figuring

Ion figuring played a critical role in the figuring of the segments for the Keck telescopes. Assuming the same areal density of material to be removed for CELT segments implies removing $30^2/(2 \times 10^2) = 4.5$ times the material removed from both Keck primaries. To reduce the cost we need technology development to improve the removal rate. Potential avenues include improved ion guns, multiple ion guns, oblique (rather than normal) incident beams, more energetic beams, different element beams, and multiple stations operating in parallel.

If the technology can be substantially improved, we can consider the attractive possibility of replacing stressed mirror polishing with ion figuring for introducing the asphere. Stressed mirror polishing requires labor intensive processes of attaching, adjusting, and removing the stressing fixture and levers. Such a fabrication option might consider beginning with hexagons and planetary polishing spherical surfaces into the already cut hexagons. The average material removed for Keck segments was about 1.2×10^{12} microns^3 per segment (segment area = 2.1 m^2) equivalent to an average height of 0.57 microns. The average volume of material removal required to introduce the astigmatism in the CELT segments is about 9.3×10^{12} microns^3 per segment (segment area = 0.65m^2) equivalent to an average height of 14 microns. Thus the total volume to be removed is $(9.3/1.2)(1080/72) = 116$ times greater for CELT than for both Keck primaries.

Using current commercial capabilities and with a Gaussian beam with $\sigma = 0.025$ meters, removing about 1×10^{12} microns^3 requires about two days of ion figuring. Removing 9.3×10^{12} microns^3 requires an estimated 17 days. Thus with no improvement in the removal rate and assuming six figuring chambers operating in parallel, it would require about 8 years to figure 1080 segments. An improvement in the removal rate by about a factor of 4 would make this approach attractive for CELT.

If we use Stressed Mirror Polishing to remove only the residual errors, then about 2 years with a single gun suffices.

Warping Harness

The final figure of the Keck segments are achieved by applying forces through the segment support to deform the surface small amounts. A system of 30 leaf springs is manually set using in telescope test results and strain gauges on the leaf springs. Although the Keck adjusting system issomewhat awkward and time consuming, we believe that it is prudent to design some system for adjusting the segment figures in the telescope. There are multiple sources of errors that might be introduced between the end of the fabrication production processing and the use of the segments in the telescope. The current design of the Gran Telescopio Canarias calls for six springs on the back of each of 36 segments that apply forces under remote control. Remote control of a CELT system will be required. The exact number of and range of forces will be determined by the errors expected from the fabrication, support, and installation of the segments.

7. SEGMENT TESTING OPTIONS

The critical importance of measuring the surface during the fabrication motivates our creating a detailed plan and a technology development program for segment testing. We want to measure segments in both circular and hexagonal shapes. We will need to design supports for both shapes that can be used during the fabrication process. The deformations induced by these supports will be minimized in the design, measured to high precision, and used in the test data analysis. Ideally, for the final measurements the support will be identical to that used in the telescope.

Segment Surface Figure Measurements

For the fabrication of the Keck segments we used a profilometer during the polish-test cycles. The profilometer was a linear array of LVDTs on a graphite-epoxy beam. It was stored on a reference surface, and for measurements was placed on the segment surface and manually or robotically clocked in azimuth. For the CELT in-process measurements, we envision using a two-dimension array of LVDTs. This will receive from above either a reference surface or the segment. Readout, correction for support-induced deformations, and a fit to polynomials will be scripted to provide rapid feedback to the polishing process.

For surface measurements at the conclusion of polishing and after ion figuring we envision using an interferometric test. This test must accommodate the large aspheric departure while maintaining an accuracy of 15nm rms surface error or better. For segmented optics, the relative segment curvatures must be controlled accurately (about 1 part in 10^5).

There are several possible interferometric tests that could be used to measure the aspheric surface of each segment. We describe three options here, list some advantages and disadvantages, and select an initial preference for our baseline fabrication process.

To achieve the highest measurement accuracy and efficient processing, for each option we assume phase-shifting interferometry is used.

Major sources of errors in interferometric tests include 1) metrology errors in the test configuration 2) turbulence in the light path, 3) vibration-induced position changes between optical elements, 4) differential optical path errors due to the non-common path of the measurement and reference wavefronts, 5) distortion of the aspheric mirror coordinate system in the detector plane, and 6) magnification calibration errors. The sensitivity to all these errors define and distinguish the three options.

To significantly reduce the sensitivity to sources 1 and 2, all options use converging lenses to reduce beam distances to less than about 6 meters. To significantly reduce sources 5 and 6; we assume all options reduce the number of measured fringes. The three options are distinguished by the technique used to achieve this.

      Option A Uses computer generated holograms.
      Option B Uses the test configuration geometry of the final segment use.
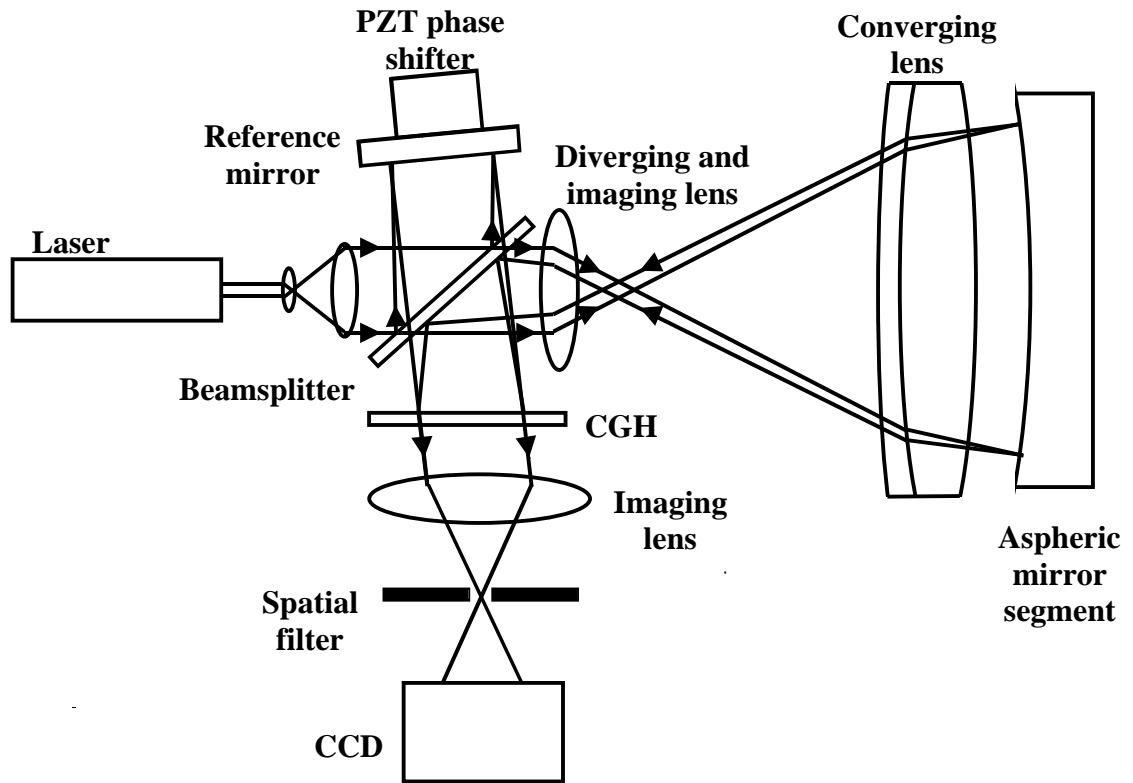   Option C Uses a tilted lens to create a canceling astigmatic wavefront.

Figure 3: Configuration for measuring an aspheric mirror segment using a computer generated hologram (CGH). The CGH is designed to null the aspheric surface departure in the image of a specific mirror segment.

Option A. Computer Generated Holograms

A computer-generated hologram (CGH) is created that contains a stored reference wavefront specific to the mirror to be measured. When the CGH is illuminated by an image of the wavefront reflected from the actual mirror, the first-order diffracted wavefront is combined with a reference plane wave. The resultant interference pattern contains the difference, or error in the mirror surface (Malacara, 1992).

Figure 3 shows a typical test configuration. The expanded wavefront from the laser is divided by the beamsplitter with one wave going to the reference mirror and the other to a diverging lens. The spherical wavefront from the diverging lens is incident on the converging lens and segment where the aspheric departure from a sphere is imposed on the phase of the reflected wavefront. The reflected wavefront is imaged onto the CGH by the same converging lens and diverging lens. The wavefront is diffracted by the CGH into several orders. The order corresponding to the virtual image of the planar wavefront that was used to compute the CGH is the only order that passes through the spatial filter and is re-imaged onto the CCD.

The waveftont reflected from the reference mirror is shifted in phase, transmitted by the CGH as the zero order and passes through the spatial filter to interfere with the first wavefront on the CCD. The intensity frames, captured as the phase is shifted, are analyzed to obtain the surface figure of the mirror segment.

Advantages and disadvantages include:
   a. The measurement includes the errors in the beamsplitter, reference mirror, diverging/imaging lens and converging lens. The reference mirror and beamsplitter can be measured separately for compensation. However, the error due to the sheared beam paths in the diverging/imaging and converging lenses cannot be directly measured using a

spherical standard. They can be calculated with lens design codes, but this does not account for fabrication errors.

    b.   It is difficult to independently confirm that the CGH has been written correctly. Fractional errors in the CGH line spacings introduce the same fractional error in units of the testing wavelength.

    c.   There is no in-situ method to measure the distortion introduced by the diverging/imaging lens.

    d.   Alignment of the CGH and aspheric mirror to the optical axis of diverging/imaging lens is critical, as are the proper conjugate positions.

    e.   There are 183 unique aspheric prescriptions for CELT. It may be impractical to make an individual CGH for each one. Perhaps about ten CGHs could cover the full range with sufficient accuracy.

    f.   Fiducials must be used to ensure the asphere location in the segment, the magnification, and the distortion are known. Conventional fiducials placed on the mirror surface will not be imaged with sufficient resolution due to the spatial filter.

The setup in Figure 3 is not the only configuration for CGH interferometry. The CGH can also be placed close to, and not in an image plane of the optic under test. This is not an option for CELT segments due to their size. Other configurations project the CGH onto the aspheric mirror segment, use null optics to simplify the CGH or place the reference surface in close proximity to the optics under test to reduce the effects of air turbulence (Burge, 1995).

Phase-shifting Diffraction Interferometers

Options B and C both use a phase-shifting diffraction interferometer (Sommargren *etal.* , 1996 and 1999). Light from a laser is coupled into a single-mode optical fiber (diameter ~ 3 microns). At the exit face the light is diffracted, producing a near-perfect spherical wavefront. Part of this spherical wavefront passes through a converging lens. The lens introduces the power required to greatly reduce the size of the test configuration. After reflecting from the surface under test the wavefront interfers with a reference spherical wave from the same or another fiber and the interferogram is imaged in a CCD camera. The reference is moved axially using a piezo-electric actuator to scan the relative fringe phases.
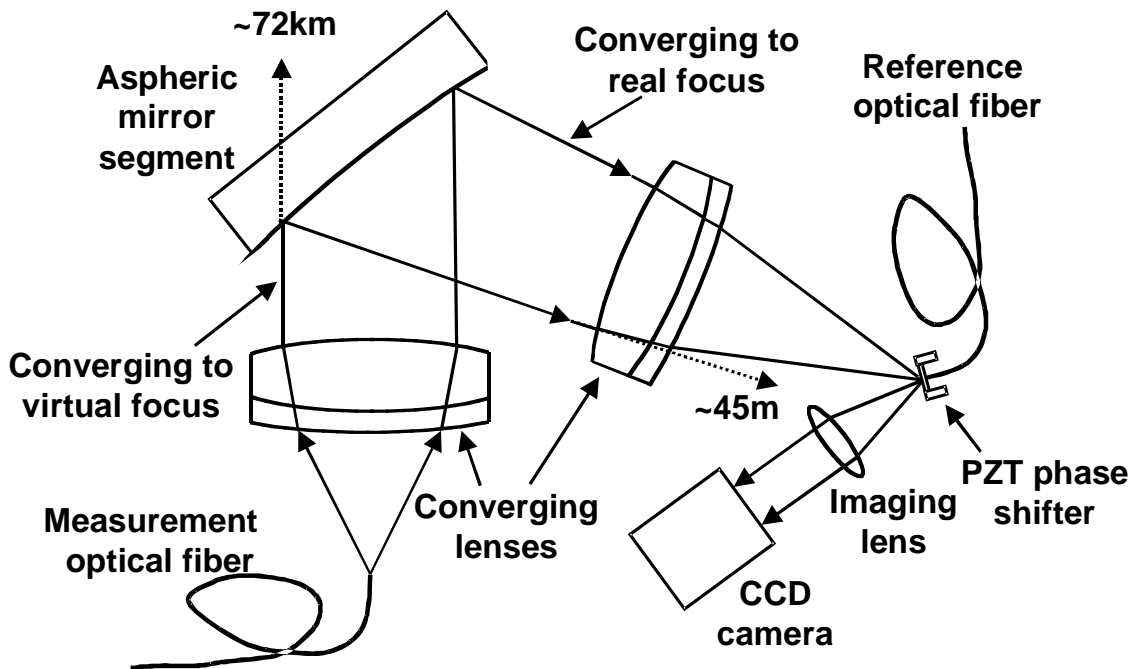

Figure 4: Configuration for measuring an aspheric mirror segment as it is functionally used in CELT. A second converging lens is used to make this a single pass test.

Option B.   **Functional Test**

A functional test measures the segment in the configuration that will used in the telescope. The test geometry itself cancels the asphericity seen by the interferometer.

The segment is tested in a single-pass configuration using a second identical converging lens with a phase-shifting diffraction interferometer (Figure 4). In this configuration the measurement and reference wavefronts are generated by diffraction from two distinct fibers. The spherical wavefronts from the fibers are focused at the conjugate points of the segment surface $f1,2 = [\ 1 \pm (-\ K)^{1/2}\ ]\ [\ k/(K+1)\ ]$. For k = 90 meters and K = −1.0025, $f1,2 = $ ~72km, ~ 45 m. The wavefront reflected from aspheric mirror segment is brought to focus at the real image point by the second converging lens where it is reflected, phase shifted, and combined with the diffracted wavefront from the reference fiber.

Advantages and disadvantages include:
     a.   The number of optical components is minimal, minimizing the possible sources of error.
     b.   The surface figure measurement also includes the errors in the two converging lenses. However, the effects of the converging lenses can be measured directly for compensation using a spherical standard because there is no wavefront shear in this testing configuration.
     c.   Distortion cannot be measured with masks because of shadowing due to non-normal illumination.
     d.   All 183 unique aspheric mirror segments cannot be measured with this method due to physical interference between the two converging lenses. For 1-meter size segments, only segments with R greater than about 7.5m can be accommodated without making the test setup greater than about 6 meters. One of the other testing approaches would have to be used for the inner segments (about 250 of 1080 segments).

This approach is limited in its applicability and is not a primary candidate for testing. However it could serve as a cross-check for either of the other methods.

Option C.   **Tilted Lens**

The primary aberration on every aspheric segment is astigmatism. The dominant wavefront aberration introduced by tilting a lens is also astigmatism. By proper design of the converging lens to minimize spherical aberration, the converging lens can be used to offset the astigmatism in the aspheric segments so that measurements are made at an interference null. Interferometers operating under this condition introduce the smallest errors because there is no shear between the measurement and reference wavefronts.

Figure 5: Configuration for measuring an aspheric mirror segment using a phase-shifting diffraction interferometer with a variable tilt converging lens. The tilt is varied to match the astigmatism of the segment, producing a near-null interference pattern.
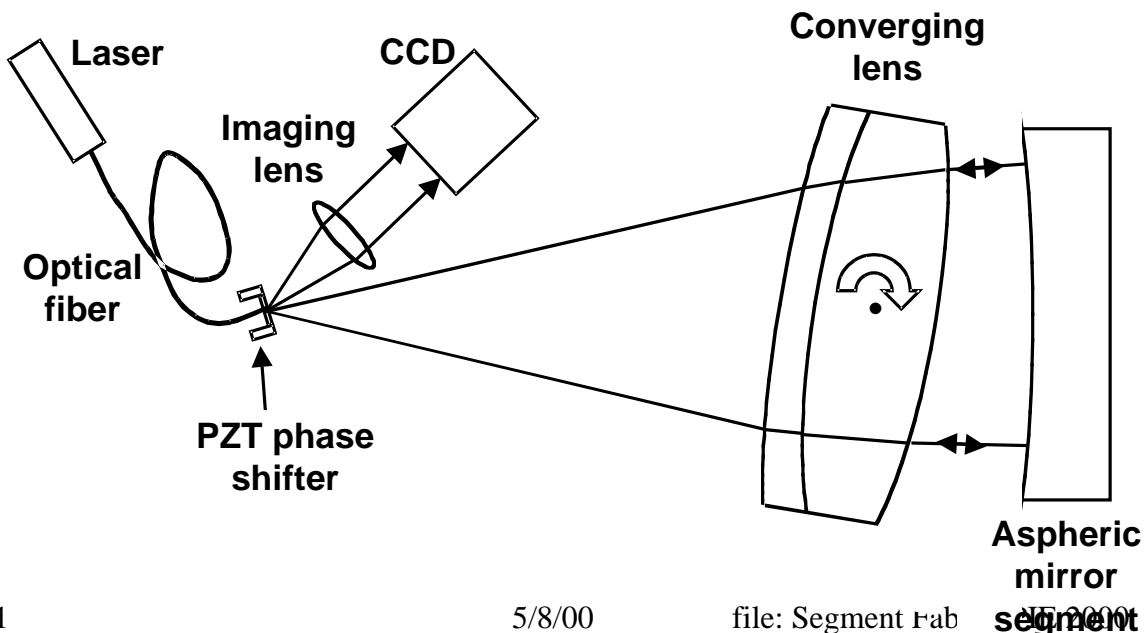
One possible configuration is shown in Figure 5. Light from the laser is coupled to a single mode optical fiber. At the exit face the light is diffracted, producing a near-perfect spherical wavefront. Part of this spherical wavefront passes through the tilted converging lens and is incident on the aspheric mirror segment where any surface figure errors are imposed on the phase of the wavefront. Upon reflection it passes back through the converging lens and comes to focus on the end of the fiber where it is reflected, phase shifted, and combined with part of the directly diffracted spherical wavefront. The imaging lens brings these wavefronts to the CCD at the image plane of the aspheric mirror segment. Data acquisition and analysis are the same as described for the CGH.

Advantages and disadvantages include:
  a. The number of optical components is minimal, reducing the possible sources of error.
  b. The surface figure measurement also includes the error in the converging lens. However, this can be measured independently using a spherical standard because there is no wavefront shear in this testing configuration.
  c. Position, magnification, and distortion can be measured directly by accurately positioning a calibrated fiducial mask on the asphere, the surface imaged on the CCD.
  d. Tilt calibration of the converging lens is critical. This can be checked with inner segments, where the astigmatism is small, by measuring a segment with and without tilt. The same check can be used for outer segments with a known differential tilt between two measurements on the same segment.
  e. Tilting can address all 183 unique aspheric prescriptions in one setup. The spacing between the converging lens and mirror will also require measurement to accommodate the range of the segment radii of curvatures.
  f. Knowing the fiber -end positions relative to the tilted lens is critical to achieving the tolerance on C_{20}.

We have made a preliminary design of this lens. We assume a focal length required to reduce the focal distance to about 6 meters. A single lens with spherical surfaces generates about 80 microns of spherical aberration. Traditionally this is removed by using a doublet. We believe that it will be easier to fabricate instead a singlet with an aspheric and a spherical surface. Our initial design (not yet optimized) has the following prescription.

Surface	diameter (m)	radius (m)	conic	A6 [coefficient of r^6] (m^{-5})
Sphere	1.016	75.924	0	0
Asphere	1.016	-3.175	-0.60925	2.00×10^{-5}

Thickness = 0.080 meters , material = BK7 (n = 1.51) $\Rightarrow$ focal length = ~ 6.5 meters

We have ray traced the performance of this lens both alone and in the test configuration with various segments. As this lens is tilted, the astigmatism and spherical wavefront aberrations generated in a single pass grow quadratically with angle and coma grows close to linear. In the double-pass configuration used in the test, the lens-induced astigmatism and coma cancel those terms in the segment-reflected wavefront. For a segment at R = 15 meters, the remaining aberrations (δC_{22}, δC_{31}, δC_{33}, δC_{40}, δC_{42}, and δC_{51}) in the wavefront have 0.036 microns rms, and thus are easily measured with the phase-shifting interferometer. A tilt angle of 2.45 degrees is required for this cancellation.

Testing Error Budget

To create a test error budget we have calculated the sensitivity of the wavefront to relative motions of the three test elements. We assumed the segment is fixed and varied the positions and angles of the lens and the fiber end. These sensitivities are calculated in Appendix 1. Using these sensitivities we budgeted the errors shown in the table below. This budget is an initial estimate and will be refined as better estimates are made of the cost and the performance of the test equipment. The errors are added in quadrature.

Segment Error budget

	rms wavefront (nanometers)	allowed element position error
Total	40	
C_{20}	28	
Fabrication	20	
Test	20	
δz_{fiber}	14	6 microns
δz_{lens}	14	6 microns
C_{22} and above	28	
Fabrication	20	
Test	20	
δx_{fibet}	0	-
δy_{fibet}	10	170 microns
δx_{lens}	0	-
δy_{lens}	10	170 microns
θ_{x_lens}	10	6 arc sec
θ_{y_lens}	0	-
θ_{z_lens}	10	120 arc sec
interferometry	5	(see Sommargren, 1999)

Test option C is attractive in its simplicity and its ability to measure all segments with a single setup. However, the results are highly sensitive to the test geometry. We propose to use fringe-counting interferometers to control the test element positions and angles to achieve the tight tolerances in the above table. In addition, we will need to measure precisely and accurately the lens wavefront error. A set of tests using one or more reference surfaces will be made to periodically to confirm the test geometry.

8. SEGMENT CUTTING AND CORING

Cutting the Hexagon

The circular blanks for Keck were polished using stressed mirror polishing and then cut into the final hexagonal shape. Two tools were available for cutting; a diamond saw and an abrasive-loaded water jet. Water jet cutting tests through 75 mm thick segments failed to meet our error tolerance; the cut surface needed to be within an envelope ± 0.3 mm of the design cut plane. Near the bottom of the test cut the jet wandered beyond this allowed envelope. We used a diamond saw to cut all the Keck segments.

The baseline CELT segments are thinner (45 mm), and there is now vastly more experience with water-jet cutting. Thus water-jet cutting may be attractive for CELT. In the coming year our understanding of the historical experience will be updated, tests may be made, and cost comparisons will be made.

For Keck we attempted to have blanks free of internal stress with a required mean stress birefringence less than 3 nm/cm. Even with this stringent requirement, the release of stresses by cutting resulted in surface deformations of order 1 micron. This then defined the goal for stressed mirror polishing; doing much better than this was an un-necessary expense.

Drilling Holes

The fabrication of the Keck segments required 60 holes to be drilled in the back of each segment. Thirty-six for whiffletree supports and twelve for sensor mounting were 18 mm in diameter and 39 mm deep. A central radial-support hole was is 254

mm in diameter and 56 mm deep. An additional eleven holes were used for installation and alignment fiducials. Most of the holes were acid etched to remove fractured material and relieve local stress.

Our goal for CELT is to minimize the holes to be drilled. Sensor designs that do not require holes are being considered (Mast and Nelson, these proceedings). We are also working to design both axial and radial supports that can be bonded to the conve surface.

9. BASELINE FABRICATION PLAN

The baseline plan for CELT segment fabrication is essentially that used for the Keck segments, with some modifications to reduce costs. The Keck fabrication process is shown in the Table in Section 4 above. We believe that using the technology of planetary polishing combined with stressed mirror polishing will substantially reduce costs. The baseline plan calls for a point-diffraction interferometric test of the segments that can be used for all segment types. Our goal for the segment support structure (not described in this paper) is to minimize the number of holes required. The goals of the Technology Development Program discussed below is to provide an accurate estimate of the costs of the required processes.

10. TECHNOLOGY DEVELOPMENT PROGRAM

We are planning a series of contracts and staff recruitment to begin several technology development activities. These will include:

- Design, construct, and test a stressing fixture
- Planetary Stressed Mirror Polish of one or more segments
- ImporoveIon figuring removal rates
- Design, construct, and test a prototype segment support system
- Design, construct, and test a prototype interferometric test facility
- Measure and/or calculate sensitivities, create a detailed test error budget
- Design and test a warping harness system

Appendix 1. Sensitivities for Test Option C.

Since we express the testing error budget in terms of rms wavefront errors, it is useful to expand the wavefront in a series of Zernike polynomials with coefficients C_{nm}. The polynomials are defined below with the corresponding rms wavefront, W_{rms}, over a hexagon.

Zernike polynomial	W_{rms} / C_{nm} over a hexago
$Z_{20} = 2\rho^2 - 1$	0.510
$Z_{22} = \rho^2 \cos 2\theta$	0.357
$Z_{31} = (3\rho^3 - 2\rho) \cos \theta$	0.299
$Z_{33} = \rho^3 \cos 3\theta$	0.324
$Z_{40} = 6\rho^4 - 6\rho^2 + 1$	0.409
$Z_{42} = (4\rho^4 - 3\rho^2) \cos 2\theta$	0.287
$Z_{51} = (10\rho^5 - 12\rho^3 + 3\rho) \cos \theta$	0.281

To calculate the effects of relative motion of the test elements we assume the segment is fixed and vary the positions and angles of the lens and the fiber end. The figure below defines the coordinate system.

center of primary ●
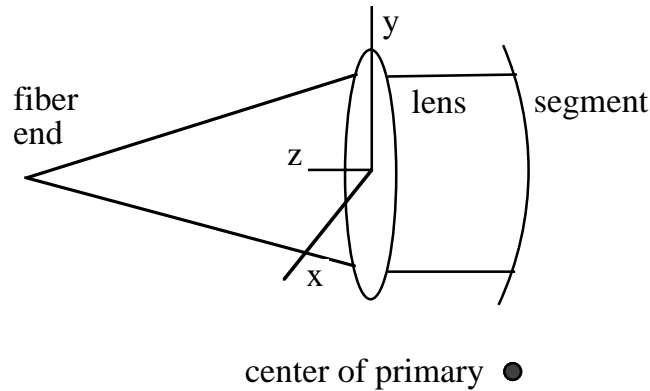
Lens

$\delta\theta_{x\_lens}$ This is the tilt used to create the astigmatism in the wavefront. We have used ray tracing of the test configuration to calculate the wavefront variations as a function the lens tilt angle.
Astigmatism and spherical aberration grow quadratically, and thus they are most sensitive for R = 15 m.

$dC_{22} / d\theta_x$ (R = 15 m) = 16.0 microns / degree
$dC_{40} / d\theta_x$ (R= 15 m) = 0.026 microns / degree

Coma changes almost linearly and has a maximum sensitivity for R = 0.

$dC_{31} / d\theta_x$ = 0.20 microns / degree

Other aberrations are small. Their variation over the range of expected lens-angle errors is negligible.
The rms wavefront error is dominated by astigmatism

W_{rms} (microns) = ($dC_{22} / d\theta_x$) 0.357 $\delta\theta_{x\_lens}$ = $\delta\theta_{x\_lens}$ (radians) / 16,900

$\delta\theta_{y\_lens}$ $dC_{22} / d\theta_x$ = 0

$\delta\theta_{z\_lens}$ This rotates the x-axis that is used to generate C_{22} , and thus generates C_{2-2}.

$W_{rms} = (\sqrt{6}/(12k^3)) KR^2a^2 \delta\phi [1 + a^2/4k^2]^{1/2}$ (Nelson, 1985) $\delta\phi = \delta\theta_z$
W_{rms} (microns) = 17.4 $\delta\theta_z$ (radians)

δx_{lens} This corresponds to an error in θ_y. The desired test configuration has $\theta_y = 0$, and there the sensitivity vanishes; $dC_{22} / d\theta_y = 0$

δy_{lens}	This will be the sum of both δR for segment and δy_{fiber}. For radial motion of the segment $W_{rms} = (\sqrt{6}/(4k^3)) \, KR \, a^2 \, \delta R \, [1 + a^2/36k^2]^{1/2}$ (Nelson,1985) $\Rightarrow W_{rms} = \delta R / 286,000$. W_{rms} (microns) $= (dC_{22} / d\theta_x) \, 0.357 \, \delta\theta_{x\_lens} = \delta\theta_{x\_lens}$ (radians)/ 16,900
δz_{lens}	The advantage of the reduced test size is gained at the expense of an increased sensitivity to the axial spacing in the test. As the segment array radius varies from R = 0 to 15 meters, the distance from the fiber to the lens (~ 5.5 meters) changes quadratically over a range of 1.75 millimeters.
	Assume the converging spherical wave at the fiber end has a radius of r. Then the wavefront Zernike amplitude $C_{20} = a^2/(4r)$, the amplitude variation $\delta C_{20} = a^2/(4r^2) \, \delta r$, and the corresponding rms wavefront over a circle is $W_{rms} = \delta C_{20} / \sqrt{3}$. Since wavefronts both leaving and returning to the fiber are affected, the final wavefront error $W_{rms} = 2 * a^2/(4R^2) \, \delta r / \sqrt{3}$. For a = 0.508 mm and r = 5.5 meters, $W_{rms} = 2.4 \times 10^{-3} \, \delta z_{fiber}$.

Fiber end

δx_{fiber}	Fiber motion in this direction corresponds to tilting the lens about the y axis. The desired test configuration has $\theta_y = 0$, and the sensitivity to angle vanishes; $dC_{22} / d\theta_y = 0$.
δy_{fiber}	This fiber motion corresponds to tilting the lens about the x axis. Using $dC_{22} / d\theta_x$ (R=15m)= 16 microns / degree and $W_{rms} = (dC_{22} / d\theta_x) \, (\delta y_{fiber} / r) \, 0.357 = \delta y_{fiber} / 16,900$, where r = 5.5 meters, yields $W_{rms} = \delta y_{fiber} / 16,900$.
δz_{fiber}	This is the same as δz_{lens}.

REFERENCES

Burge, J.H., "Application of computer-generated holograms for interferometric measurement of large aspheric optics," Proceedings of the SPIE, **2576**, pp. 258-269 (1995).

Chanan, G. A. and Sirko, E., "Design Issues for the Active Control System of the California Extremely Large Telescope (CELT)," Proceedings of the SPIE, this conference (2000)

Malacara, D., ed., *Optical shop testing* (2nd ed.), (Wiley, New York, 1992), Chapter 15.

Mast, T. S., and Nelson, J. E. , "Segmented Mirror Control System Hardware for CELT," Proceedings of the SPIE, this conference (2000)

Nelson, Gabor, Hunt, Lubliner, and Mast, *Applied Optics*, 19, 2341, 1980

Nelson, J. E. "Fabrication and Alignment Tolerances for Segments and Sensors," Keck Observatory Report No. 32 (1985)

Nelson, J. E., "Design Concepts for the California Extremely Large Telescope (CELT)," Proceedings of the SPIE, this conference (2000)

Sommargren, G.E., "Phase shifting diffraction interferometry for measuring extreme ultraviolet optics," *OSA Trends in Optics and Photonics* Vol. **4**, Extreme Ultraviolet Lithography, Kubiak and Kania, eds. (Optical Society of America, Washington, DC, 1996), pp. 108-112.

Sommargren, G.E., Phillion, D.W., Campbell, E.W., "Sub-nanometer interferometry for aspheric mirror fabrication*,"* *Precision Science and Technology for Perfect Surfaces*, Proceedings of the 9th International Conference on Production Engineering, Y. Furukawa and T. Mori, eds., pp. 329-335 (1999).